Epitaxial film growth of the charge-density-wave conductor $Rb_{0.30}MoO_3$ on $SrTiO_3(001)$

A. J. Steinfort, H. S. J. van der Zant, A. B. Smits, O. C. Mantel, P. M. L. O. Scholte, and C. Dekker
Delft Institute of Microelectronics and Submicron Technology (DIMES), Department of Applied Physics, Delft University of Technology, P.O. Box 5046, NL-2600 G A Delft, The Netherlands
(Received 29 October 1997)

Thin films of the charge-density-wave compound $Rb_{0.30}MoO_3$ (blue bronze) have been grown on $SrTiO_3(001)$ substrates. The films have been analyzed with atomic force microscopy and x-ray diffraction. The growth initially proceeds in the three-dimensional island growth mode (Volmer-Weber mode) with dropletlike islands that are highly uniform and fully relaxed. Epitaxial growth is observed: the fourfold symmetry of the $SrTiO_3(001)$ surface results in four crystallographic orientations. Thick films show cluster formations that differ in size and form from the islands that appear at the initial stage of growth. They are larger and have an asymmetric shape with clear facets. X-ray diffraction on thick films shows a decrease of both the in-plane and out-of-plane texture. The data are explained with a simple model that involves blue bronze layer growth over the facets of the clusters. The model indicates that the crystalline correlation length perpendicular to the charge-density-wave axis is smaller than the dimensions of the grains. The implications of the model on the electrical transport are discussed. [S0163-1829(98)06916-1]

I. INTRODUCTION

In quasi-one-dimensional conductors a phase transition may occur to a collective ground state in which the charge density is periodically modulated.[1,2] Both inorganic and organic materials have demonstrated this ordered charge-density-wave (CDW) state up to temperatures of several hundreds of degrees kelvin, including room temperature. In equilibrium, the CDW is pinned to impurities and conduction only occurs by quasiparticles that are excited above the energy gap. In the low bias dc resistivity, the CDW state shows up as a Peierls[3] transition from metal-like behavior at high temperatures to semiconducting behavior at low temperatures. When a moderate electric field is applied (of the order of 1 V/cm), however, the CDWs can slide collectively. The collective CDW motion leads to strongly nonlinear conduction, coherent current oscillations, and mode locking at resonant frequencies.

The sliding motion of CDWs shows many similarities with transport in superconductors, with the role of current and voltage reversed. For the collective CDW current, a current-frequency relation exists similar to the ac Josephson relation between voltage and frequency in superconductors. Thin-film devices with Josephson junctions are very important in both fundamental studies and applications of superconductivity. Such devices are unexplored for CDW systems due to the absence of a thin-film CDW technology. Various properties, e.g., the extremely high dielectric constants (up to 10^8) and the mode locking, are potentially important in this respect.

The CDW state has been studied extensively in bulk crystals for which the dimensions are much larger than the phase coherence length of the CDW. This coherence length is typically of the order of micrometers along the direction of the CDW chains. We have recently reported the first thin-film growth of a CDW compound.[4,5] In this paper we focus on a more detailed study of epitaxial growth of thin $Rb_{0.30}MoO_3$ (blue bronze) films on $SrTiO_3(001)$ substrates. We find that films grow in the island growth mode until full coverage of the surface. For thicker films, overgrowth of $(\bar{2}01)$ slabs occurs over regular cluster facets, thus limiting the correlation length. Films were investigated by means of atomic force microscopy (AFM) and x-ray diffraction.

The compound $Rb_{0.30}MoO_3$ belongs to the blue bronzes[6] $A_{0.30}MoO_3$ with A=K, Rb, or Cs. Its crystal structure is monoclinic, space group $C_{2/m}$ with 20 formula units in the unit cell. It has a layered type structure in which the slabs are built up from units containing ten distorted MoO_6 octahedra. The Rb atoms are positioned in between the slabs. The blue bronze lattice dimensions are given by $a=18.536$ Å, $b=7.556$ Å, $c=10.035$ Å, and $\beta=118.52°$.[7] Single crystals of blue bronze grow as platelets elongated in the b direction forming large $\{\bar{2}01\}$ crystal facets parallel to the slabs. Blue bronze exhibits a Peierls transition at 182 K.

In our films blue-bronze growth mainly proceeds in the $(\bar{2}01)$ direction. For this growth direction, the in-plane rectangular blue bronze lattice net is formed by the b axis and the [102] lattice vector. The mismatch between the b axis of blue bronze and twice the principal axis of $SrTiO_3(001)$ is 3.3%. In the perpendicular in-plane direction, the mismatch between the [102] blue bronze and five times the principal axis of the substrate is 1.4%. Previous scanning electron microscopy (SEM) studies[5] have shown that grains grow mainly in two perpendicular directions oriented along the principal axes of the $SrTiO_3$ substrate. No systematic study on the growth mechanism has been performed yet.

II. EXPERIMENTAL DETAILS

Blue-bronze films were deposited on $SrTiO_3(001)$ substrates by pulsed-laser deposition. By x-ray diffraction, the vicinal angle of the $SrTiO_3(001)$ substrates is estimated to 0.5° or less. No influence of these miscut angles on the film growth is observed.[8] Before mounting, the $SrTiO_3(001)$ substrates with typical sizes of $5\times5\times0.5$ mm^3 are cleaned with

organic solvents. Substrates are then glued with silver paint on a heater block that is situated opposite to the target at a distance of 4.7 cm. A polycrystalline $Rb_{0.30}MoO_3$ target is placed in a pulsed-laser beam. The illuminated area is about 5 mm^2. The background pressure in the deposition chamber is 10^{-6} Torr. During deposition the target rotates and deposition takes place in an oxygen atmosphere. To obtain single-phase blue-bronze films the substrate temperature is kept between 375 °C and 500 °C and the oxygen pressure between 100 and 175 mTorr. Films were grown with thicknesses ranging from 1.5 to 1000 nm. Film thicknesses ranging from 300 to 1000 nm were determined by measuring the depth profile across a cut through the film with a Tencor Instruments α-step 200 profilometer. Thinner films were obtained by adjusting the deposition time. More details about the film growth have been presented elsewhere.[4,5]

After deposition, various analysis techniques have been used for characterization of the blue-bronze films such as AFM, transmission electron microscopy, scanning electron microscopy, scanning tunneling microscopy (STM), optical microscopy, and x-ray diffraction. In this paper we discuss in detail the results obtained from AFM and x-ray diffraction. AFM was done with a Nanoscope III in air at room temperature.

The diffraction experiments on films with a thickness from 300 to 1000 nm were carried out with a four-circle diffractometer. The Cu K_α x-ray beam was taken from a standard laboratory source run at 20 mA and 40 kV. Slits were used to define the primary beam and the acceptance angle of the detector. The width of the primary beam in the scattering plane was 0.10°, and a Ni filter was used to eliminate the K_β contribution in the wavelength spectrum.

The x-ray measurements on two blue-bronze films with a thickness of 2 nm were performed on the vertical scattering diffractometer at the BW2 wiggler beamline in HASYLAB (DESY Hamburg). The photon energies used for the diffraction experiments at the two samples were 8.6 and 9.0 keV, respectively. The angle of grazing incidence was kept constant and equal to 0.5°. All diffraction measurements were performed in air at room temperature.

III. EXPERIMENTAL DATA

A. Initial stage of growth

The initial growth of blue bronze on $SrTiO_3(001)$ has been studied on films with a thickness between 1 and 10 nm. The film thickness is equivalent to the thickness of a continuous film with the same amount of material. The data presented here were taken on films with an equivalent layer thickness of 2 nm. A typical AFM image is shown in Fig. 1(a) in which 3D island nucleation is clearly visible. The typical length scale of the dropletlike-shaped islands is 150 $\pm$50 nm. Their height is about 10 nm. The sample in Fig. 1(a) was grown at 440 °C and the island density is about 30 μm^{-2}. We have systematically studied the initial stage of growth as a function of growth temperature and deposition rate. Island growth dominates in all cases. The density of the islands varies only slightly with deposition temperature or deposition rate.

More information about these ultrathin films is obtained by means of synchrotron x-ray diffraction. In particular, the

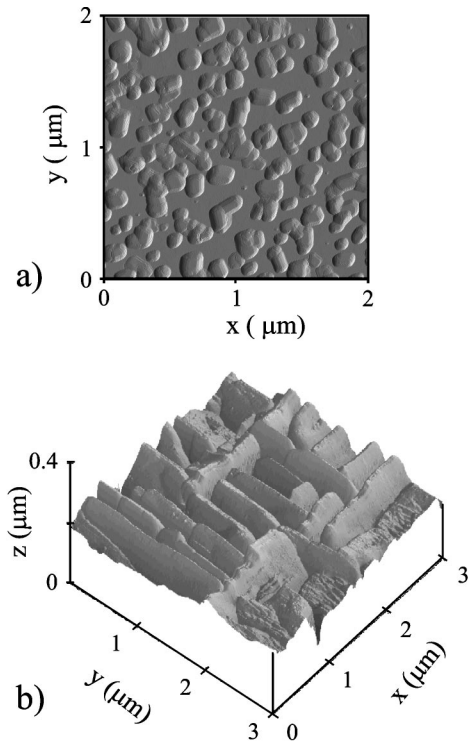

FIG. 1. AFM images of the surface of a blue-bronze film on $SrTiO_3(001)$. (a) Small islands are observed for film thicknesses of 2 nm, whereas in (b) for a film thickness of 300 nm, the surface is covered with much larger, uniformly shaped clusters.

film-substrate relation and the crystalline quality have been investigated. The film-substrate relation is determined from the in-plane and out-of-plane orientation of the crystal axes of both the substrate and the adlayer. The crystalline film quality is inspected with respect to the correlation length, the strain, and the texture. Measurements have been performed on two samples grown at 375 °C and 410 °C, which gave similar results.

The out-of-plane growth direction for blue bronze is $(\bar{2}01)$ only, which means that the layers grow plane-parallel to the surface. The orientation of the in-plane b axis in the adlayer has been determined from the intensity distribution on the (020) in-plane circle. This intensity profile describes all possible directions of the b^* axes. In Fig. 2(a), the profile at the (020) circle is shown in which the substrate is oriented such that the principal axes are along $\varphi = 0°$ and $\varphi = 90°$. The background signal is due to scattering from Vaseline used to mount the sample on the diffractometer. The four maxima in the (020) intensity profile correspond to orientations of the b axes parallel to the principal axes of the substrate.

To estimate the crystalline quality in the film, the width and the position of several independent reflections have been inspected. In general, the tangent width of the reflections (i.e., the width of the reflections along a circle in the plane of the surface) is due to a combination of a correlation length reduction and a crystalline orientation distribution. A finite-size effect results in a broadening independent of the radial position. An orientation distribution leads to a broadening with a linear dependence on the radial distance. The tangent widths of the blue-bronze (0 2n 0) reflections with $n = 1$, 2,

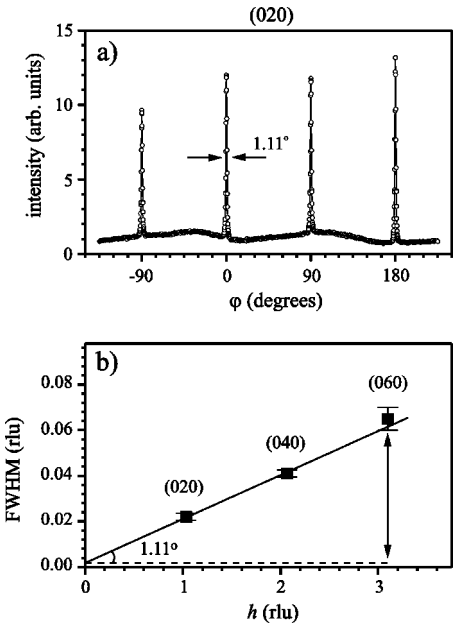

FIG. 2. X-ray-diffraction measurements from a 2-nm-thick film. (a) The scattering profile recorded on the in-plane (020) circle showing the preferred crystalline orientations. (b) The width (in $SrTiO_3$ rlu) of the (0 2*n* 0) reflections along a circle in the plane of the surface. From the slope and the offset of the linear fit through the data points the in-plane orientation distribution and the particle size are estimated.

and 3 are shown in Fig. 2(b) as a function of the radial distance in reciprocal space. The distances are expressed in $SrTiO_3$ reciprocal lattice units (rlu) with h parallel to the blue-bronze b^* axis and k in the in-plane direction perpendicular to it. The linear fit through the data points is shown as a solid line. The slope of this solid line corresponds to the orientation distribution, and from the intersection with the y axis the island size can be estimated. As can be seen in Fig. 2(b), the peak broadening is almost entirely due to an orientation distribution of 1.11°. The intersection of the linear fit with the y axis corresponds to an island size of 200 nm. As the intersection is close to the origin, the relative error is large, but the estimate of 200 nm equals the size of the islands as deduced from AFM images. Apparently, the islands are monocrystalline.

The strain in the film has been deduced from the positions of the in-plane (020) reflection together with thirteen independent reflections. Strain shows up as an asymmetric peak profile or in a shift of the peak position. No asymmetry or positional shifts with respect to the bulk reflection positions have been found up to 0.1%. This implies that the initial islands are fully relaxed. The relaxed, monocrystalline crystal formation on the surface with an orientation distribution of over 1° suggests a very weak film-substrate bonding. In spite of this weak bonding, heteroepitaxial film growth is observed: the films are oriented with the (201) slabs parallel to the substrate surface and the b axis oriented along the substrate principal axes.

B. Thick $Rb_{0.30}MoO_3$ films on $SrTiO_3$(100)

Continuation of the deposition of blue bronze leads to a full coverage of the surface at a layer thickness of about

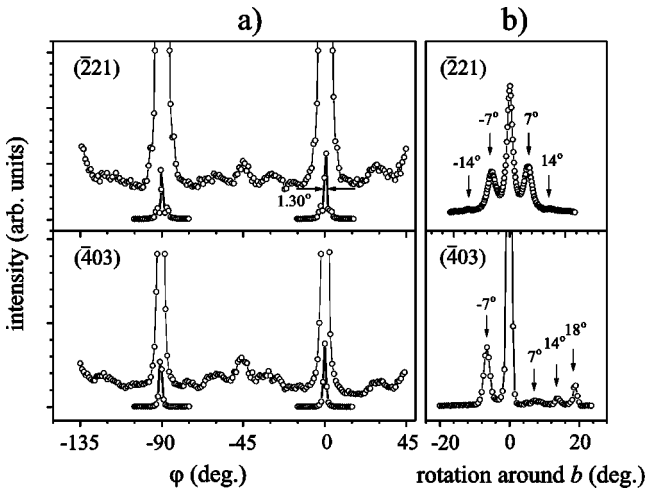

FIG. 3. The intensity distribution from a 300-nm-thick film recorded through the main (221) and the (403) reflections. In (a) the circle parallel to the surface is scanned showing four main in-plane crystalline orientations. In (b) the intensity is recorded by rotating the sample around the b axis.

10–50 nm. At coverages equivalent to 15 nm and more, AFM images show the formation of larger, uniformly shaped clusters. A typical AFM image of a 300-nm-thick film is shown in Fig. 1(b). This film is grown at the same temperature and deposition rate as the film in Fig. 1(a). Clearly, the density of the clusters is significantly less than the island density at the initial stage of growth. In contrast to films at the initial stage of growth, we find that both the island density and grain sizes of the thick films are strongly temperature dependent. Island density varies from 10 μm^{-2} at 375 °C to 3 μm^{-2} at 440 °C. Grain sizes range from 0.3 $\times 0.5$ μm^2 at 375 °C to 1×5 μm^2 at 440 °C. In general, thick films consist of grains that are about 10–100 times larger than the islands at the initial growth stage.

Grains in thick films have a form that is very different from the dropletlike shape. As can be seen in Fig. 1(b), elongated grains grow in two perpendicular directions. Section analysis on the height profiles shows that the clusters are asymmetrically bound by facets along the long side. The facet planes are well defined and make preferred angles with the substrate. The angles of more than 1000 facets have been measured by the AFM and plotted in a histogram [see Fig. 5(b)]. From this histogram the preferred angles are estimated to be 7°, 14°, 18°, 22°, 30°, 32°, and 39°. Angles larger than 50° were impossible to measure by AFM because of convolution between the tip and the surface profile.

The film texture and relative orientations of the islands have been studied by means of x-ray diffraction. Measurements are performed on films with a thickness ranging from 200 to 1000 nm. In general, the in-plane and out-of-plane texture decreases by increasing the film thickness. The out-of-plane growth direction of the blue-bronze layers remains mainly (201). Only a minor part of the film is (403) oriented as has been estimated from an out-of-plane θ-2θ x-ray scan.

The in-plane orientation of the (201) clusters has been investigated from the intensity profiles on the surface-parallel circles through the (221) and the (403) reflections. An example of the scattering profiles is shown in Fig. 3(a). The substrate principal axes are oriented along the $\varphi = 0°$

and the $\varphi = 90°$ directions. For clarity, the intensity profiles around the maxima are shown on a larger intensity scale. The similar shape of the profiles shows the azimuthal orientation distribution of the (201) clusters. The four main intensity maxima in Fig. 3(a) result from clusters that are oriented with the *b* axes along the substrate principal axes. The width of the maxima is 1.3°, slightly more than the width of the peaks in Fig. 2(a). In general, we find that for thick films the in-plane width of the maxima is substantially more than 1° typically, it varies between 2° and 7°. In addition to the main orientations along the substrate axes, intermediate orientations are present that make an angle of 27° and 45° with the substrate principal axes. The width of these maxima is about 10°. Both the broadening of the peaks and the observation of additional orientations indicate a reduced in-plane texture for thick films.

The out-of-plane orientation shows a similar trend as found for the in-plane orientation, less texture with increasing films thickness. All additional out-of-plane orientations, however, have the *b* axes in the plane of the surface. In Fig. 3(b) the profiles through the main (221) and (403) reflections are shown. The *x* axes in these plots indicate a rotation around the *b* axis. The profiles clearly contain several side peaks next to the main reflection. We have checked that the side peaks do not result from a superperiodicity. The main reflection belongs to a (201)-oriented material and the side peaks result from blue bronze with tilted (201) planes. The tilt angles equal 7°, 14°, and 18°. In the conventional unit cell description, most of these orientations do not result in low-index planes parallel to the surface except for the peak near 18°. Rotation of the (201) slabs over 18° around the *b* axis results in (403)-oriented material, in agreement with the θ-2θ scans.

With synchrotron x-ray diffraction, it is in principle possible to measure facet angles if the facets are well defined and have dimensions of tens of nanometers or larger. Cluster faceting results in the appearance of intensity rods in reciprocal space parallel to the facet normal[9] analogous to the appearance of crystal truncation rods as a result of the presence of a crystal surface. An example is shown in Fig. 4. Three profiles are shown, recorded in the surface-parallel direction along a principal axis at different heights in reciprocal space. The central peak in the profiles is the crystal truncation rod as a consequence of the surface. On both sides of the central peak, minor peaks are visible. These side peaks form a line of intensity that makes an angle of 55° with the surface. The peak broadening due to the orientation distribution prohibits the observation of facet angles smaller than 40°. The diffraction measurements can therefore not confirm the presence of facets with angles smaller than 40° as observed in the AFM studies.

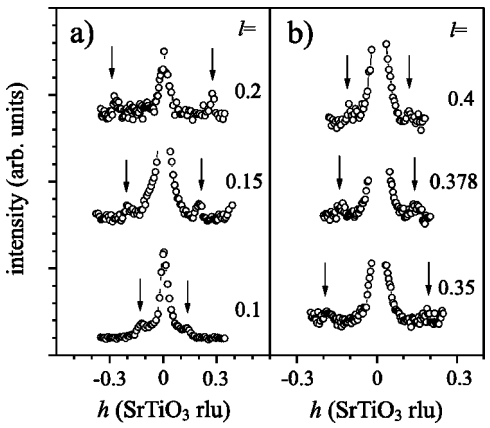

FIG. 4. The lateral intensity profile of a 300-nm-thick blue-bronze film recorded at different heights in reciprocal space. Extra reflections are visible on both sides of the rod through the blue bronze (201) as a result of the facets on the blue-bronze clusters. The reflections run in a direction 55° with the surface. In (a) the reflections coincide at the blue bronze (020) at $l = 0$ and in (b) they coincide at blue bronze (221) at $l = 0.473$.

IV. DISCUSSION

Film growth on $SrTiO_3(001)$ initially proceeds in the 3D island growth mode (Volmer-Weber mode). The typical island size is 50–200 nm with an island height of about 10 nm. The islands are monocrystalline and show clear epitaxial behavior: the fourfold symmetry of the substrate surface results in four crystallographic blue-bronze orientations. Islands grow in the (201) direction with the *b* axis along the principal axes of the substrate. The relaxed state of the islands indicates a weak film-to-substrate bonding. This weak bonding may also be responsible for the in-plane mosaic spread of 1.1°. At an average film thickness of 10–50 nm, the surface is fully covered with islands. Between the closed-packed islands, grain boundaries will appear as a result of the discrepancy between the unit nets of the substrate surface and the film. The grain boundaries will limit the correlation length to the size of the islands. At higher coverages a change in the growth appears. Larger, highly uniform, elongated clusters start to form with dimensions 10–100 times larger than the initial islands. The grain density is considerably smaller than at the initial stage of growth. In both the in-plane and the out-of-plane direction the number of preferred orientations and the mosaic spread increases.

Our observations suggest three distinct stages of growth. In the initial stage, small monocrystalline islands nucleate at the substrate surface. Growth of these islands proceeds until full coverage. In the second stage, overgrowth of large clusters bounded by well-defined facets occurs. Since these clusters cover several uncorrelated initial islands, a decrease in the in-plane texture is expected. This decrease is, for instance, evident in the observed increase of the in-plane mosaic spread. The third stage of growth is characterized by growth of (201) slabs over the facets.

The model for the second and third stages of growth can be made more quantitative by describing the clusters with a modified unit cell. This cell is built up from unit blocks defined by the in-plane [102] and *b* axis, and the *c* axis. In this new description, several (h 0 l) facets can be formed, with only small values of h and l. For example, the 14° facet corresponds to a (201) facet with a terrace width of two unit cells followed by a step of one unit cell height. The (100) facet corresponds to the 55° faceting as measured with x-ray diffraction. The angles of 7°, 14°, 18°, 22°, 30°, and 39° as observed in AFM measurements are identified as (104), (102), (101), (403), (101), and (401) facets, respectively. Note that this model predicts the clusters to be asymmetric when viewed along the *b* axis [Fig. 5(a)]. The growth of

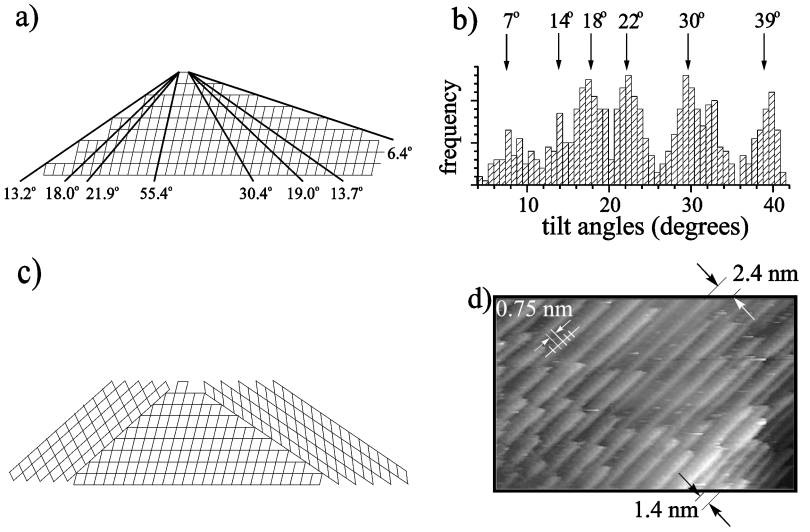

FIG. 5. A model for the cluster growth. The second stage of growth as described in the text is illustrated in the upper panel. Various facet angles are schematically shown in (a), which correspond to the angles determined from AFM data (b). The third stage of growth is illustrated in the lower panel. The growth of (201) slabs over the cluster facets is schematically shown in (c). The overgrowth is confirmed by STM images of a cluster (d) showing different periodicities perpendicular to the *b* axis.

$(\bar{2}01)$ slabs over the faceted grains is schematically shown in Fig. 5(c). The angles between the (201) slabs and the surface are consistent with the x-ray diffraction data [Fig. 3(b)].

The overgrowth of the slabs is also confirmed by STM measurements.[10] In Fig. 5(d) an STM image of a cluster is shown. In this image periodic line structures are observed. In these lines the *b*-axis periodicity is present with a period of 0.75 nm. The lines are the end points of tilted (201) slabs as illustrated in Fig. 5(c). The periodicity perpendicular to the *b* axis is therefore determined by the facet angle over which overgrowth occurs. The horizontal distance between (201) slabs is equal to $d_{(\bar{2}01)}/\sin(\text{tilt angle})$ with $d_{(\bar{2}01)}=0.83$ nm. In Fig. 5(d) we observe periodicities of 2.45 and 1.43 nm between the lines. These distances correspond to tilt angles of 22° and 39°. We have made many STM images of blue-bronze clusters. Most of the clusters contain a periodicity in a direction perpendicular to the *b* axis. In all cases, we could identify a low-index facet angle that corresponds to the observed period.

The overgrowth results in a correlation length that is smaller than the cluster size. This conclusion is consistent with our electrical transport measurements on blue-bronze films. In general, we find an energy gap that is lower than the observed values (520 K) in bulk blue bronze. Films grown on $Al_2O_3(012)$ show a systematic decrease of the energy gap with decreasing grain size. Films grown at high temperatures with large grains have an energy gap close to the bulk value. For films with submicron grains, the gap is reduced by 30%. Such a dependence is absent for films grown on $SrTiO_3(001)$: no matter how large the grain size, the apparent gap deduced from electric transport measurements is almost constant (around 400 K). Extrapolation of the results obtained on the $Al_2O_3(012)$ substrates then yields that the grains seen by SEM on $SrTiO_3(001)$ must consist of smaller clusters.

V. CONCLUSIONS

Highly textured films are grown on $SrTiO_3(001)$ substrates. At the initial growth, heteroepitaxial monocrystalline islands form with a weak substrate-film bonding. The blue bronze is fully relaxed, and orients with the in-plane *b* axis to the principal axes of the substrate. An orientation distribution of 1.1° around these directions is observed. On thick films, grains are considerably larger and the orientation spread increases. The major part of the grains remains oriented with the *b* axis along the principal axes of the substrate. A minor part of grains have additional orientations of 27° and 45° with respect to the $SrTiO_3\langle 100\rangle$. In the out-of-plane direction, the thick films show additional orientations. The *b* axis remains oriented in-plane, but besides the surface-parallel (201) slabs, a tilt of the slabs is observed. A correlation between the faceting of the clusters and the preferred out-of-plane orientations is found. The data are fully explained with a model including growth of (201) slabs over facets of the clusters. The model indicates that the correlation length perpendicular to the *b* axis is smaller than the dimensions of the grains. This observation is consistent with electrical transport data, which show that the energy gap measured in films grown on $SrTiO_3(001)$ substrates is largely independent on the apparent grain size as deduced from SEM pictures.

ACKNOWLEDGMENTS

The authors would like to thank P. W. F. Rutten and C. A. W. Bal for their careful AFM work, and K. R. Koops for the support by the STM measurements. We also want to thank M. Nielsen and J. Baker for the assistance on the diffraction experiments at the DESY synchrotron in Hamburg. This work has been supported by The Netherlands Foundation for Fundamental Research on Matter (FOM).

[1] G. Grüner, *Density Waves in Solids* (Addison-Wesley, Reading MA, 1994).
[2] P. Monceau, in *Electronic Properties of Inorganic Quasi-One Dimensional Compounds*, edited by P. Monceau (Reidel, Dordrecht, 1985), Vol. 2.
[3] R. Peierls, *Quantum Theory of Solids* (Oxford University Press, Oxford, 1955), p. 108.
[4] H. S. J. van der Zant, O. C. Mantel, C. Dekker, J. E. Mooij, and C. Træholt, Appl. Phys. Lett. **68**, 3823 (1996).
[5] O. C. Mantel, H. S. J. van der Zant, A. J. Steinfort, C. Dekker, C. Træholt, and H. W. Zandbergen, Phys. Rev. B **55**, 4817 (1997).
[6] C. Schlenker, J. Dumas, C. Escribe-Filippini, and H. Guyot, in *Low-Dimensional Electronic Properties of Molybdenum Bronzes and Oxides*, edited by C. Schlenker (Kluwer, New York, 1989), pp. 159–257.
[7] W. J. Schutte and J. L. de Boer, Acta Crystallogr., Sect. B: Struct. Crystallogr. Cryst. Chem. **49**, 579 (1993).
[8] A. J. Steinfort, Ph.D. thesis, Delft, The Netherlands, (1998).
[9] A. J. Steinfort, P. M. L. O. Scholte, A. Ettema, F. Tuinstra, M. Nielsen, E. Landemark, D.-M. Smilgies, R. Feidenhans'l, G. Falkenberg, L. Seehofer, and R. L. Johnson, Phys. Rev. Lett. **77**, 2009 (1996).
[10] A. J. Steinfort and H. S. J. van der Zant (unpublished).